Study on Polymer-Surfactant Interactions for the Improvement of Drug Delivery Systems Wettability

I. De Simone,[a] N. Coceani,[b] R. Farra,[b] S. M. Fiorentino,[b] G. Grassi,[c] R. Lapasin,[b] D. Hasa,[a] B. Perissutti,[a] M. Grassi,[b] and D. Voinovich[a,*]

[a]Department of Chemical and Pharmaceutical Sciences, University of Trieste, Piazzale Europa 1, I-34127, Trieste, Italy

[b]Department of Engineering and Architercture, Piazzale Europa, I-34127, Trieste, Italy

[c]Department of Life Sciences, Cattinara University Hospital, Strada di Fiume 447, I-34149, Trieste, Italy

Original scientific paper
Received: June 8, 2012
Accepted: July 24, 2012

One of the possible causes of failure of the mechanochemical activation of poorly soluble drugs relies on the scarce drug wettability. Indeed, the mechanochemical process comports the disposition of drug nano-crystals and amorphous drug, generated by the destruction of original drug macro-crystals, on the surface of the carrier (acting as stabiliser), usually represented by crosslinked polymeric particles. Accordingly, the scarce drug wettability can reduce the beneficial action of mechanochemical activation (nano-crystals and amorphous drug are characterised by a higher solubility with respect to the original macro-crystals). In this light, this paper is focussed on the use of surfactants for the increase of delivery system (drug plus carrier) wettability. In particular, the surfactant-polymer systems are characterised for what concerns their bulk and surface properties. This allows to select the best surfactant and to experimentally verify its effect on the release kinetics of a poorly soluble and wettable drug.

Key words:
Wettability, mechanochemical activation, surfactant, surface characterization.

Introduction

Oral dosage form represents the most common route for drug administration into human body because it leads to a better patient compliance and it is very versatile for what concerns dosing conditions [1,2]. Unfortunately, however, oral dosage form can be not so effective due to poor drug solubility in aqueous environments such as physiological media. Indeed, solubility is an important requirement to ensure good body absorption after oral administration. In other words, pharmaceutical system bioavailability, defined as the rate and extent to which the active drug is absorbed from a pharmaceutical form and becomes available at the drug action site[3], is heavily influenced by drug solubility that becomes the absorption rate determining step for class II drugs (good permeability, poor solubility) according to the Amidon biopharmaceutical classification[4]. While an ideal drug (100% bioavailability) gets the site of action unmodified without undergoing metabolism and elimination pathways, a real one, especially if slightly bioavailable, has to be administrated in high dose to ensure a minimum effective concentration at the site of action. In this case, consequently, the appearance of dose-depending side effects can be probable. A possible strategy to improve solubility and, thus, bioavailability, without modifying drug chemical structure, strictly connected to therapeutic properties, is to act on drug physical properties. Indeed, it is well known[5] that the smaller the drug crystal, the higher its solubility in a liquid system. This statement, a little bit intriguing, neither represents a paradox, nor confutes thermodynamic theory. Indeed, at fixed temperature and pressure, drug solubility in a solvent is a unique value descending from the principle of minimal energy that translates into the equality of all species chemical potential in the liquid and solid phase. In virtue of the minimal energy principle, however, this definition of solubility implicitly assumes that the solid phase is represented by crystals of infinite dimension, this being the most stable configuration the solid phase can assume. If, on the contrary, it were possible to realise the equilibrium between a liquid phase and a solid one made by very small crystals (nano-crystals or, more precisely, crystallites), it can be thermodynamically demonstrated that drug solubility is dependent on crystals size[5]. However, as nano-crystals represent a metastable condition for the solid phase and they

*Corresponding author: e-mail: vojnovic@units.it; Tel: 39 040 558 3106; Fax: 39 040 52572

tend to assemble together to get the most stable infinite crystal condition, it is not experimentally possible to achieve a two phases "*equilibrium*" in presence of a nano-solid phase. Nevertheless, in the presence of particular stabilising agents, the metastable nano-crystals condition can be stabilised and, at least for a limited period, it is possible to take advantage of the increased solubility[6]. Obviously, the amorphous drug condition can be viewed as a nano-crystal of vanishing dimension which competes the highest solubility in a solvent at fixed temperature and pressure[7]. In this sense, both nano-crystals and amorphous phase represent an activated state for the drug.

It is now clear the necessity of choosing a proper stabilising agent to have a reliable and effective delivery system able to take advantage from the above discussed nano-crystals property. Depending on drug physicochemical characteristics, particular polymers (typically crosslinked amphiphilic ones) can stabilise nano-crystals and amorphous drug phase by trapping them inside their three-dimensional network or on their surface. Indeed, due to polymer – drug interactions and to the physical presence of the polymeric chains (drug macro-crystals can form on condition that the dry network meshes be sufficiently wide), macro-crystals formation, at least in the dry state, is practically hindered[5,6]. On the contrary, when polymeric particles come into contact with the external liquid environment, solvent diffusion inside the polymeric network gives rise to the swelling process and to drug dissolution, coupled with nano-crystals and amorphous drug re-crystallisation into macro-crystals. The presence of the solvent and the enlarged dimensions of the network meshes make negligible the polymer stabilising action. Practically, release kinetics develops as the dissolving drug were characterised by a decreasing solubility, spanning from a higher value to a lower one, characteristic of the macro-crystal[8,9]. As re-crystallisation is not instantaneous, on average, drug release kinetics is improved[5, 6].

Although different techniques exist to disperse the drug inside the polymeric network (solvent swelling[6,10] and supercritical fluids[11,12], for example), in form of very small crystals ranging from the nano-scale to the virtually zero-dimensional crystals representing by the amorphous state, co-grinding proved to be a reliable strategy[13–15]. Moreover, it has the considerable advantage of not requiring the use of solvents whose elimination from the final formulation can often represent a very expensive and delicate stage. Indeed, solvent must be eliminated without extracting the drug and without modifying drug distribution inside the polymer as it is well known that this distribution can sensibly affect the release kinetics[16,17]. Unfortunately, however, when the drug is highly hydrophobic and its abundance in the co-ground system is relevant (drug-polymer ratio ≥ 1/3 w/w) delivery system wettability can be very low[18]. In this case, despite of good drug activation, bioavailability can be depressed and the use of surfactants becomes unavoidable. Accordingly, aim of this work was to study polymer-surfactant interactions in order to select the best candidate able to confer the highest wettability to the carrier system (polymer) which, in turn, reflects on the improvement of the whole drug-polymer system wettability. Firstly, polymer-surfactant bulk properties were studied in order to measure surfactant solubility in the polymeric bulk phase. Then, attention was focussed on the polymer-surfactant system surface properties. Indeed, it is essential to evaluate whether surfactant disposes at the solid surface or not as system wettability modifications are only due to the superficial surfactant fraction. Finally, *in vitro* release tests were used to evaluate the macroscopic effect of surfactants on release kinetics.

Materials and methods

In the light of its amphiphilic nature and of its wide use as drug nano-crystals stabilizer[5,6,10,15], polyvinyl-pyrrolidone (PVP) was chosen as polymeric carrier. In particular, two PVP types were used: the linear one (K90, Kollidon BASF) and the crosslinked one (polyvinyl-pyrrolidone, PVP-CL-M.) Investigated surfactants were sodium lauryl sulfate (SLS, anionic, Sigma Aldrich), tetradecyl trimetyl ammonium bromide (TTAB, cationic, Sigma Aldrich) and poloxamer 407 (Lutrol, not ionic, Sigma Aldrich). All of them are approved for oral administration and frequently employed in formulations[19,20]. Nimesulide (Helsinn, PambioNoranco, CH), a typical non-steroidal anti-inflammatory drug (NSAID), was considered as model drug as it belongs to the Amidon class II (low solubility and high permeability drug)[4] and for its low wettability[21].

Determination of bulk properties

K90 aqueous solutions (7% w/w) containing different surfactant amounts, were prepared, poured in aluminium pans and there dried (drying overnight under air flux followed by 40 minutes at 80°C in a oven) to get films. Differential scanning calorimetry (Perkin Elmer DSC 7, Perkin Elmer, Norwalk, CT) was then led on these films to determine the polymer-surfactant phase diagram and, thus, surfactant solubility in the polymer reach phase (temperature calibration was made, at the

same heating rate, using Hg and In as standards). In order to eliminate water traces, films underwent a first heating step led at 10°C/min (SLS, from 50°C to 190°C; TTAB, from 20°C to 110°C; Lutrol from 20°C to 180°C) followed by an analogous cooling. Then, 1 minute isotherm (SLS 50°C; TTAB 20°C; Lutrol 20°C) preceded the definitive heating (SLS, up to 200°C; TTAB up to 190°C; Lutrol up to 190°C) at 10°C/min. DSC scans were performed under N_2 stream (20 cm^3/min) to prevent samples from oxidation.

DSC analysis was firstly addressed to determine the variations of polymer glass transition temperature (T_g). Indeed, T_g, characteristic of each amorphous polymer, decreases with increasing surfactant concentration because of surfactant plastic agent action. Then, first order transitions (melting), characteristic of crystalline surfactants, were considered in order to individuate the eventual presence of a surfactant reach phase, being the polymer reach one the only phase existing until surfactant solubility in the polymer was not exceeded.

X-Ray diffraction analysis (Stoe 500, Siemens, Germany, equipped by a Cu Kα source (40KV, 20 mA)) allowed getting information on possible film crystalline structure due to the presence of a surfactant reach phase.The scanning angle ranged from 5 to 35° of 2θ, steps were of 0.05° of 2θ, and the counting time was of 5 s/step.This technique was used to support what found by means of DSC analysis.

Determination of surface properties

K90-surfactant films, characterised by different surfactant mass fraction (up to 7% for SLS and up to 9% for TTAB. This characterisation was not performed in the case of Lutrol for the reasons exposed in the results and discussion section), were prepared by casting the polymer-surfactant aqueous solution on a glass support. Water evaporation was performed under controlled conditions in order to get a homogeneous surface free from cracks and bubbles. Films surface properties were firstly determined by measuring the contact angle (tensiometer G10, Kruss, GmbH, Hamburg, D; sessile drop technique) relative to a polar solvent (distilled water) and an apolar one (diiodomethane). Then, in order to verify the existence of one or two phases on film surface, the Cassie-Baxter equation[22] was used:

$$\cos\theta_a = f_1 \cos\theta_1 + f_2 \cos\theta_2 \quad (1)$$

where θ_a is the apparent contact angle measured on film surface while f_1 and f_2 are the surface fractions occupied by the two phases, each one characterized by its own contact angle (θ_1 and θ_2). As, obviously, $f_1 + f_2 = 1$, eq.(1) becomes:

$$\cos\theta_a = f_1 (\cos\theta_1 - \cos\theta_2) + \cos\theta_2 \quad (2)$$

which expresses a linear dependence of $\cos\theta_a$ on f_1. Thus, if the experimental trend of $\cos\theta_a$ is not linear with f_1, it is not possible that two superficial phases exist on film surface.

To further characterize films surface properties, their solid-liquid (γ_{sl}) and solid-vapor (γ_{sv}) surface tensions were determined. At this purpose, Young equation[23] was used:

$$\gamma_{lv} \cos\theta = \gamma_{sv} - \gamma_{sl} \quad (3)$$

where θ is the contact angle and γ_{lv} is the liquid-vapor surface tension competing to the probe liquid used to wet film surface. As in eq.(3) γ_{sv} is unknown, its value was estimated according to the Wu approach[24]. This approach relies on the hypothesis that γ_{sv} is the sum of two contributes:

$$\gamma_{sv} = \gamma_{sv}^d + \gamma_{sv}^p \quad (4)$$

where γ_{sv}^d is the dispersional component and γ_{sv}^p is the polar component. In addition, assuming that the mean interaction potential relative to the two immiscible phases (the liquid and the solid phase, in our case) is given by the harmonic mean of the interaction potential of each phase, Wu got the following relation:

$$\gamma_{lv}(1+\cos\theta) = \frac{4\gamma_{sv}^d\gamma_{lv}^d}{\gamma_{sv}^d + \gamma_{lv}^d} + \frac{4\gamma_{sv}^p\gamma_{lv}^p}{\gamma_{sv}^p + \gamma_{lv}^p} \quad (5)$$

where γ_{lv}^d and γ_{lv}^p are, respectively, the dispersional and the polar component of γ_{lv}. While γ_{lv}^d, γ_{lv}^p and γ_{lv} can be found in literature for many liquids[18], γ_{sv}^d and γ_{sv}^p are unknowns. Accordingly, their determination implies the simultaneous solution of two equations of the eq.(5) type relative to two different liquids. In so doing, the balance among equations and unknowns (γ_{sv}^d and γ_{sv}^p) is achieved as, obviously, γ_{sv}^d and γ_{sv}^p do not depend on the liquid used but they depend only on the solid film surface characteristics. In particular, in this work, two different liquids were considered: distilled water and diiodomethane. Indeed, while water is essentially polar, diiodomethane is essentially apolar. Once γ_{sv}^d and γ_{sv}^p are known, eq.(4) allows the determination of γ_{sv}. On this basis, eq.(3) yields γ_{sl} when the solid-liquid contact angle (θ) has been experimentally determined. Knowledge of γ_{sv} is not only important *per se*, but it is also essential for the determination of the film surface composition in relation to different surfactant concentration in the film bulk. Indeed, for a two components (1 = polymer, 2 = surfactant) system made up by a vapor (v) and a solid (s) phase in equilibrium, Gibb-Duhem equations hold[25]:

$$n_1^v d\mu_1^v + n_2^v d\mu_2^v = 0 \quad (6)$$

$$n_1^s d\mu_1^s + n_2^s d\mu_2^s = 0 \quad (7)$$

where n_1^v and n_2^v represent, respectively, the moles of polymer and surfactant in the vapor phase, n_1^s and n_2^s represent, respectively, the moles of polymer and surfactant in the solid phase (film) while $d\mu_1^v = d\mu_1^s = d\mu_1$ and $d\mu_2^v = d\mu_2^s d\mu_2$ are, respectively, the infinitesimal variation of polymer and surfactant chemical potential. Eqs.(6) and (7) can be coupled with the Gibb's equation pertinent to the solid-liquid interface[22]:

$$d\gamma_{sv} = -\Gamma_1^{sv} d\mu_1 - \Gamma_2^{sv} d\mu_2 \quad (8)$$

where Γ_1^{sv} and Γ_2^{sv} are, respectively, the so called excess of polymer and surfactant on the solid-vapor interface. According to the Gibb's theory[22], when Γ_i^{sv} (i = 1 or 2 in our case) is equal to zero, the surface and the bulk composition of component ith are equal, i.e, the excess (or defect) of component ith on the surface is zero. Expressing $d\mu_1$ dependence on $d\mu_2$ according to eq.(6) and substituting this expression into eq.(8), we get:

$$d\gamma_{sv} = -\Gamma_1^{sv} \frac{n_2^s}{n_1^s} d\mu_2 - \Gamma_2^{sv} d\mu_2 \quad (9)$$

or:

$$\frac{\partial \gamma_{sv}}{\partial \mu_2} = -\Gamma_1^{sv} B - \Gamma_2^{sv} \qquad \frac{n_2^s}{n_1^s} = B \quad (10)$$

Remembering the relation existing between the chemical potential and activity ($d\mu_2 = RT\, d\ln a_2$; where T indicates the absolute temperature, R is the universal gas constant and a_2 is the surfactant activity), we have:

$$\frac{1}{RT} \frac{\partial \gamma_{sv}}{\partial \ln a_2} = -\Gamma = -(\Gamma_1^{sv} B + \Gamma_2^{sv}) \quad (11)$$

As in the case of diluted solutions (surfactant concentration less than 0.1), surfactant activity (a_2) can be approximated by its concentration (c_2), eq.(11) can be approximated by:

$$\Gamma = -\frac{1}{RT} \frac{\partial \gamma_{sv}}{\partial \ln c_2} = \Gamma_1^{sv} B + \Gamma_2^{sv} \quad (12)$$

Relying on eq.(12), it is easy to verify the validity of the following relations:

$$\Gamma_1^{sv} = \frac{\partial \Gamma}{\partial B} \quad (13)$$

$$\Gamma_2^{sv} = \Gamma - \frac{\partial \Gamma}{\partial B} B \quad (14)$$

Polymer-surfactant interaction in aqueous solution

In order to investigate the polymer-surfactant interaction in liquid phase, different aqueous solution (polymer concentration = 10 mg/cm^3) with increasing surfactant concentrations (spanning from 10 to 10000 μg/ml) were prepared. Then, liquid-vapor surface tension was measured by means of a tensiometer G10 (Krűss GmbH, Hamburg, D, pendant drop technique). In the case of important interactions between the polymer and the surfactant, variations in the γ_{lv} versus $\ln(c_2)$ should be detected[26]. Both K90 and PVP-Clm were used. Obviously, in the case of PVP-Clm, we were in presence of dispersions and not of solutions due to cross-linked nature of PVP-Clm.

Preparation and calorimetric investigation of co-ground samples

Nimesulide/PVP-CL-M/surfactant physical mixture (ratio 11:32:1 (w/w)) and Nimesulide/PVP-CL-M physical mixture (ratio 11:33 (w/w) were co-ground for 2 hours in a planetary mill (Pulverisette 7, Fritsch GmbH, D)) setting the rotational speed to 530 rpm. Mill vials, made up by agate, contained seven agate balls (1 cm diameter) plus 1.5 g of physical mixture. The planetary mill was chosen as it is efficient and its dynamic behaviour, jointly with the energy transfer to co-ground materials, is well understood[27]. The co-ground material was sieved (60 mesh – 250 μm). Pure nimesulide and different co-ground systems were characterised by means of DSC. The samples were put into aluminium pans (about 6–7 mg in the case of co-ground systems and about 2 mg in the case of pure drug) and then scanned under a N_2 stream of 20 cm^3/min at a heating rate of 10 °C/min. In order to eliminate water from the co-ground materials, a four step procedure was applied: 1) heating from 20°C to 90°C 2) cooling from 90°C to 70°C 3) resting at 70°C for 2 minutes 4) heating from 70°C to 160 °C.

Release test

Drug and polymer

Release tests, performed in triplicate in not sink conditions, were led in 600 cm^3 water (V_r) at 37°C. At time zero, 200 mg of physical mixture (nimesulide/PVP-CL-M, 11:33 weight ratio, simply mixed) or co-ground systems (nimesulide/PVP-CL-M, weight ratio 11:33, mixed and then subjected to co-grinding; Nimesulide/PVP-CL-M/surfactant weight ratio 11:32:1, mixed and then subjected to co-grinding) were added to the release environment. The reason for choosing this drug-polymer ratio relies on the fact that lower ratios are not

probably connected to wettability problems due to polymer abundance. On the contrary, higher ratios would reflect in poorly stable systems due to the polymer lack.

Drug

In the case of pure nimesulide, 50 mg of drug were added to the release environment (600 cm^3 water (V_r) at 37°C). In so doing, the drug dose is the same used in the test performed on the drug-polymer system.

Operative conditions

Uniformity conditions were ensured by means of an impeller (rotational speed 200 rpm). The use of an optical fibre apparatus (HELLMA, Italy), connected to a spectrophotometer (ZEISS, Germany, wavelength 393.4 nm), allowed the determination of nimesulide concentration (C_r) without perturbing the release environment (each release test lasted 20 minutes). Moreover, this methodology allowed to easily overcome the problem connected to drug concentration measurement in presence of a dispersion of solid particles. Indeed, while the maximum nimesulide absorption occurred at 393.4 nm, the scattering effect due to polymeric particles uniformly occurred at every wavelength. Accordingly, the real absorbance related to nimesulide concentration was the difference between the absorbance measured at 393.4 nm and that measured at 500 nm (at 500 nm nimesulide does not absorb).

Results and discussion

Bulk properties

Figure 1, showing the DSC behaviour relative to K90, reveals that this amorphous polymer is characterised by an inflection with a midpoint at 174°C, attributable to its glass transition temperature (T_g), followed by a relaxation endotherm. At the same time, Figure 2 shows that two thermal events characterise the DSC pattern of SLS: the first, occurring at 87°C, represents a solid-solid transition while the second, positioned at 196°C, indicates the solid-liquid phase transition. These considerations were supported by the hot stage microscopy studies (FP 52 Mettler, Greifensee, CH, connected to a temperature controller FP 5 Mettler) (data not shown).

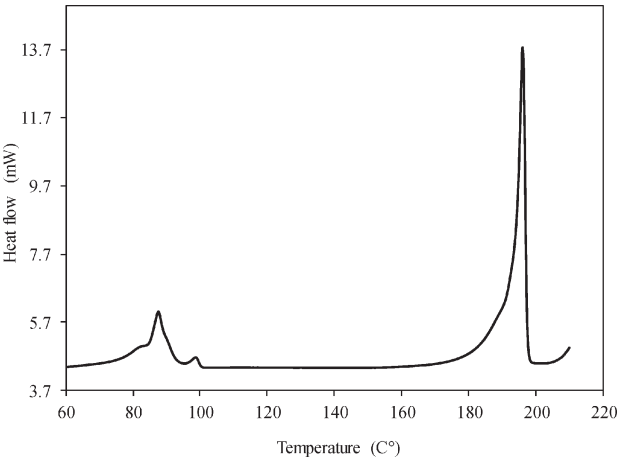

F i g . 2 – *DSC pattern of SLS. Endothermic peak is upward*

Indeed, while no liquid phase was visible at 87°C, an evident liquid phase appeared at 196°C. The information contained in Figure 1 and 2 represent the initial (0% SLS content) and final part (100% SLS content) of the K90-SLS phase diagram reported in Figure 3. Figure 3 was realised by performing a DSC analysis on different K90-SLS systems characterised by an increasing content (mass fraction X 100) of SLS[21]. Accordingly, all the thermal events characterising the different K90-SLS systems were recorded and reported in the phase diagram of Figure 3. It can be seen that, up to a SLS content of about 9%, only one phase exists and the

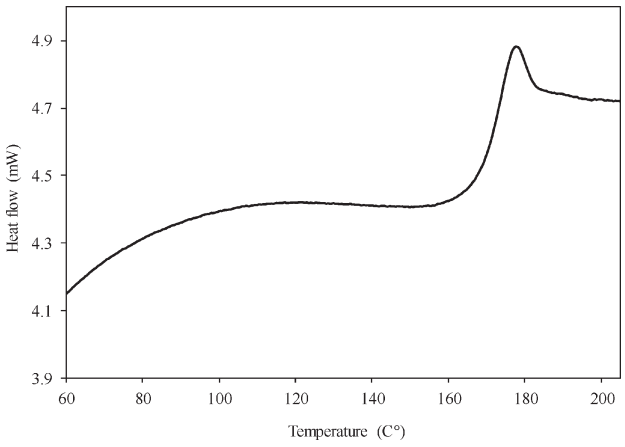

F i g . 1 – *DSC pattern of K90. Endothermic peak is upward*

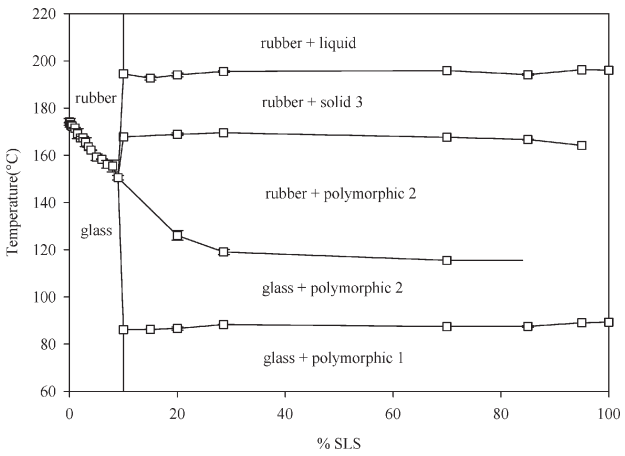

F i g . 3 – *SLS-K90 phase diagram*

increase of SLS content simply reflects into a reduction of the T_g competing to the K90-SLS system. This is reasonable as SLS, acting as a plasticizer agent, enhances K90 molecules mobility. Obviously, once temperature T exceeds T_g, the glass phase transforms into a rubber phase. As soon as SLS content exceeds 9%, DSC analysis reveals the presence of a bi-phasic system composed by a K90 reach phase and an SLS reach phase.

Indeed, other three thermal events add to the original one referring to the glass-rubber transition. Accordingly, up to ≈ 87°C (pure SLS solid-solid transition) we have the coexistence of a glass phase, rich in K90, and a solid phase, rich in SLS, denominated polymorphic 1. A temperature increase induces the transformation of the SLS-rich phase in the polymorphic 2 state while being unaffected the glass phase. Depending on the SLS content, this second biphasic region spans from ≈ 87°C to 115 – 150°C. Once this threshold is overcome, the glass phase becomes rubber while no modifications are observed in the SLS-rich phase (polymorphic 2). A further temperature increase reflects into the formation of new SLS-rich phase denominated "solid 3". This biphasic region spans between 167°C and 196°C, regardless of SLS content. As the "solid 3" phase cannot be detected in the pure SLS (no thermal event occurs around 167°C, see Figure 2) we should suppose that solid 3 is induced by the presence of K90. After 196°C, the coexistence of a rubber, K90 rich, phase and a liquid, SLS rich, phase takes place.

In order to support the existence of only one phase for SLS < 9% and the existence of two phases for higher SLS content, X-ray diffraction pattern were recorded for K90, SLS and two different K90-SLS systems (SLS = 5% and SLS = 28.6%). Figure 4 and 5 show, respectively, the comparison

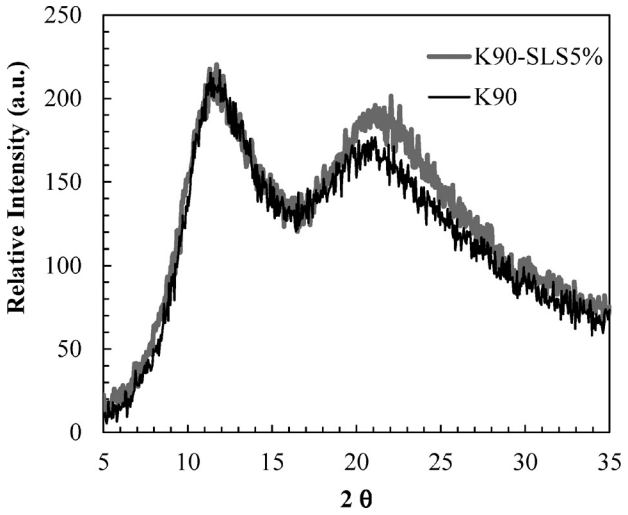

F i g . 4 – *X-rays pattern relative to K90-SLS 5% and K90 systems*

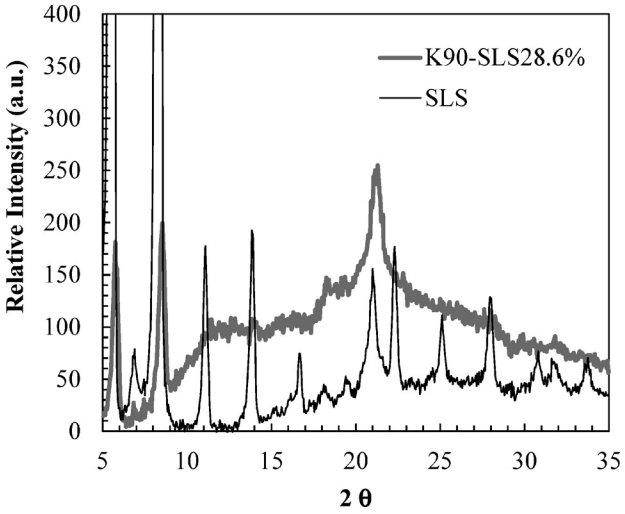

F i g . 5 – *X-rays pattern relative to K90-SLS 28.6% and SLS systems*

between the X-ray pattern relative to the couples (K90 and K90-SLS 5%) and (SLS and K90-SLS 28.6%).

It is clear that in the K90-SLS 5% system the peaks characteristic of SLS are not visible while a diffraction pattern very similar to that of K90 appears. This means that, in this case, no solid phase is present and only one amorphous phase exists. On the contrary, in the K90-SLS 28.6%, some of the peaks, characteristic of pure SLS, are present and this witnesses the presence of a solid phase rich in SLS. In addition, the X-ray pattern relative to the K90 rich phase is detectable.

The phase diagram relative to the K90-TTAB system, reported in Figure 6, was built according to the same procedure followed for the determination of the K90-SLS phase diagram. We can see that for TTAB contents lower than 10% only one phase exists and system T_g, correctly, decreases with in-

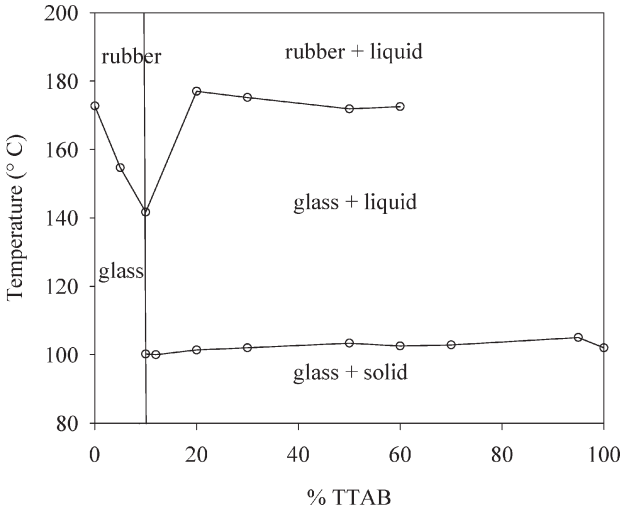

F i g . 6 – *TTAB-K90 phase diagram*

creasing TTAB concentration. Once this threshold is exceeded, a bi-phasic condition occurs: a K90 rich phase coexists with a TTAB rich phase. Indeed, the DSC trace shows the appearance of the TTAB solid-liquid transition (around 100°C) plus another peak that indicates the T_g of the K90 rich system. Accordingly, when TTAB content exceeds 10%, a temperature rise gives origin to the phase transformations reported in Figure 6. For TTAB content exceeding 60%, the phase diagram is not so clear due to the disappearance of the T_g peak. Anyway, this region is not of practical interest due to the very high surfactant content. Obviously, also in this case, the X-ray analysis, performed on three different systems (K90-TTAB 3%, 7% and 50%), revealed that only one phase exists for TTAB contents lower than 10% while a two-phase system appears for higher concentrations.

Finally, Figure 7, showing the K90-Lutrol phase diagram, makes clear that the solubility of this surfactant inside K90 is very limited (around 0.5%). Accordingly, its use in combination with K90 seemed not promising.

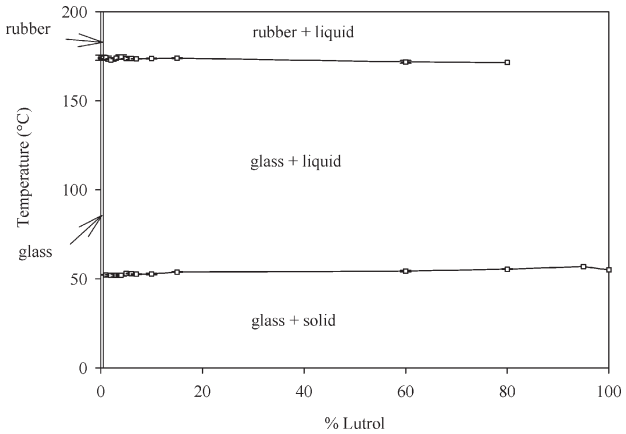

F i g . 7 – *Lutrol-K90 phase diagram*

Surface properties

Table 1 reports the water (θ_{H2O}) and the diiodomethane (θ_{CH2I2}) contact angles relative to K90-SLS films characterized by increasing amount of SLS up to 7%, i.e., just below SLS solubility in the K90-SLS system (see Figure 1). These data reveal that while the increase of SLS amount does not reflect in systematic variations of θ_{H2O}, SLS increase implies an increase of θ_{CH2I2}. In addition, it is easy to verify that the trend of cos(θ) versus %SLS (= f_1), for both water and diiodomethane, does not follows a linear trend as it should be according to the Cassie-Baxter equation (eq.(2)). Thus, we can conclude that only one phase exists at the K90-SLS film solid-vapor interface. This is in agreement with what found by means of the bulk characterization

T a b l e 1 – *Water contact angle (θ_{H2O}) ± standard deviation, diiodomethane contact angle (θ_{CH2I2}) ± standard deviation, polar (γ^p_{lv}) and dispersional (γ^d_{lv}) liquid-vapor surface tension relative to water and diiodomethane, solid-vapor surface tension (γ_{sv}), polar (γ^p_{sv}) and dispersional (γ^d_{sv}) solid-vapor surface tension relative to K90-SLS films characterized by increasing amount of SLS (mass fraction X 100). All data refer to room temperature (20–25°C).*

SLS (%)	θ_{H_2O} (°)	$\theta_{CH_2I_2}$ (°)	γ_{sv} (mJ/m^2)	γ^p_{sv} (mJ/m^2)	γ^d_{sv} (mJ/m^2)
0	55 ± 1	17 ± 1	64.2	19.0	45.2
1	46 ± 3	25 ± 1	67.1	24.0	43.0
2	56 ± 2	42 ± 2	57.0	20.6	36.4
3	60 ± 2	55 ± 3	50.8	20.7	30.1
4	55 ± 4	64 ± 3	51.2	25.0	26.2
4.5	58 ± 3	64 ± 5	49.6	23.4	26.2
5	56 ± 3	55 ± 8	52.9	22.8	30.0
7	39 ± 5	59 ± 5	61.2	33.0	28.2
data from ref 17					
H_2O	γ^p_{lv} (mJ/m^2) = 51		γ^d_{lv} (mJ/m^2) = 21.8		
CH_2I_2	γ^p_{lv} (mJ/m^2) = 1.3		γ^d_{lv} (mJ/m^2) = 49.5		

(see K90-SLS phase diagram reported in Figure 1). Table 1 also shows that, according to eq.(5), the increase of SLS reflects into a convex variation of γ_{sv} (minimum value around 4%) while the polar component (γ^p_{sv}) increases and the dispersional component (γ^d_{sv}) decreases. The addition of SLS makes the surface more hydrophilic and, consequently, more wettable by water.

On the basis of the γ_{sv} dependence on the amount of SLS (see Table 1), it was possible evaluating the excess of polymer (Γ_1^{sv}) and surfactant (Γ_2^{sv}) on the solid-vapor interface according to eqs.(12)-(14). At this purpose SLS content, expressed as mass fraction X 100, was converted into molar concentration (moles/m^3) knowing that polymer and SLS molecular weights are, respectively, 10^6 and 288.4 and that film density is, in the range $0 < \text{SLS\%} \leq 7\%$, approximately equal to 885 Kg/m^3. Thus, the resulting γ_{sv}vs. ln(c_2) curve was fitted by the following equation:

$$\gamma_{sv} = A\,(\ln(c_2))^3 + D\,(\ln(c_2))^2 + E\,(\ln(c_2)) + F \quad (15)$$

and the values of the fitting parameters were: A = 9.3, D = –110.4, E = 419.0 and F = –446.8. Relying on eq.(15), (dγ_{sv}/dln(c_2)) was determined and, consequently, Γ (see eq(12)) could be evaluated for all the experimentally tested B ($= n_2^s/n_1^s = c_2/c_1$) values. The pseudo-experimental trend of Γ versus B was fitted by the following equation:

$$\Gamma = l + m\sqrt{B} + p/B \qquad (16)$$

and the values of the fitting parameters were: l = 0.0546, m = –0.0041 and p = –0.9257.

The evaluation of the slope and intercept of the tangent to $\Gamma(B)$ in each experimentally considered B value, allowed to determine the excess of polymer (Γ_1^{sv}) and surfactant (Γ_2^{sv}) on the solid-vapor interface as reported in Figure 8. Figure 8 shows that while Γ_1^{sv} is almost zero whatever the SLS content, Γ_2^{sv} is negative for %SLS < 2% and then becomes positive. This means that the polymer surface concentration is always equal to the bulk one, while the SLS surface concentration is lower than the bulk one for %SLS < 2% and it is bigger than the bulk one for SLS ≥ 2%. Accordingly, for a bulk concentration ≥ 2%, the surfactant should exert its action at best.

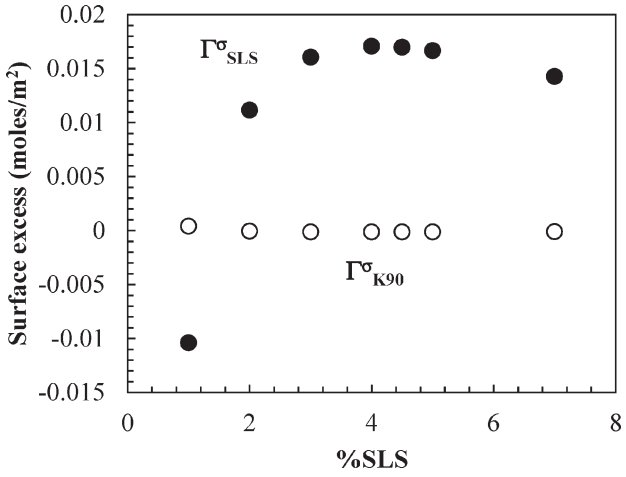

Fig. 8 – *Trend of the polymer (Γ_{K90}^{sv}) and surfactant (Γ_{SLS}^{sv}) surface excess versus the SLS mass fraction X 100*

The study of the surface properties was also performed in the case of TTAB, while it was not performed in the case of Lutrol as this surfactant showed to be almost insoluble in K90 (see Figure 7). Table 2 reports the water (θ_{H_2O}) and the diiodomethane ($\theta_{CH_2I_2}$) contact angles relative to K90 TTAB films characterized by increasing amount of TTAB up to 9%, i.e., just below TTAB solubility in the K90-TTAB system (see Figure 6).

It can be seen that the addition of TTAB implies a general reduction of θ_{H_2O} and a general increase of $\theta_{CH_2I_2}$. Data shown in Table 2 reveal, also, that the trend of cos(θ) versus TTAB% (= f_1), for both water and diiodomethane, does not follows a linear trend as it should be according to the Cassie-Baxter equation (eq.(2)). Consequently, we can conclude that only one phase exists at the K90-TTAB film solid-vapor interface. This is in agreement with what found by means of the bulk

Table 2 – *Water contact angle (θ_{H2O}) ± standard deviation, diiodomethane contact angle (θ_{CH2I2}) ± standard deviation, polar (γ_{lv}^p) and dispersional (γ_{lv}^d) liquid-vapor surface tension relative to water and diiodomethane, solid vapor surface tension (γ_{sv}), polar (γ_{sv}^p) and dispersional (γ_{sv}^d) solid-vapor surface tension relative to K90-TTAB films characterized by increasing amount of TTAB (mass fraction X 100). All data refer to room temperature (20–25°C).*

TTAB (%)	θ_{H_2O} (°)	$\theta_{CH_2I_2}$ (°)	γ_{sv} (mJ/m²)	γ_{sv}^p (mJ/m²)	γ_{sv}^d (mJ/m²)
0	55 ± 1	17 ± 1	64.2	19.0	45.2
0.5	36 ± 2	28 ± 3	71.1	29.3	41.7
1	32 ± 1	22 ± 2	74.5	30.6	43.8
2	35 ± 1	26 ± 1	72.0	29.6	42.4
3	35 ± 1	19 ± 1	73.3	28.8	44.5
5	38 ± 2	26 ± 1	70.7	28.3	42.4
7	37 ± 2	29 ± 1	70.6	29.1	41.5
9	34 ± 5	19 ± 1	73.8	29.3	44.5
data from ref 17					
H_2O	γ_{lv}^p (mJ/m²) = 51.0		γ_{lv}^d (mJ/m²) = 21.8		
CH_2I_2	γ_{lv}^p (mJ/m²) = 1.3		γ_{lv}^d (mJ/m²) = 49.5		

characterization (see K90-TTAB phase diagram reported in Figure 6). Table 2 also shows that, according to eq.(5), the presence of TTAB causes an increase of γ_{sv} but this increase seems independent on TTAB concentration (TTAB%). In addition, while the dispersional component (γ_{sv}^d) is un-affected by the presence of TTAB, the polar component (γ_{sv}^p) increases, but this increase is independent on TTAB%. As the dispersional component is always bigger than the polar one, we should conclude that the effect of TTAB on surface wettability is smaller than that of SLS, where the polar component resulted similar, if not bigger, than the dispersional one for SLS% ≥ 4%.

On the basis of the γ_{sv} dependence on the amount of SLS (see Table 2), it was possible evaluating the excess of polymer (Γ_1^{sv}) and surfactant (Γ_2^{sv}) on the solid-vapor interface according to eqs.(12)-(14). At this purpose TTAB content, expressed as mass fraction X 100, was converted into molar concentration (moles/m³) knowing that polymer and TTAB molecular weights are, respectively, 10^6 and 316.1 and that film density is, in the range 0 < TTAB% ≤ 9%, approximately equal to 1271.8 Kg/m³. As γ_{sv} is, substantially, constant with TTAB% (see Table 2) and, thus, with ln(c_2), it turns out that also Γ is constant with B. Accordingly, we found that Γ_1^{sv} = 0 and Γ_2^{sv} = 4.2*10^{-5} moles/m². This means that there is no excess of K90 on film surface, i.e. K90 surface concentration is equal to

the bulk one. On the contrary, TTAB surface concentration is bigger than the bulk one. The comparison between TTAB and SLS surface behavior indicates that for SLS% ≥ 2%, the surface excess competing to SLS is around 300 times that competing to TTAB. A further comparison between SLS and TTAB performance can be led by evaluating their behavior in aqueous solution/dispersion in presence of K90 (water soluble; 10 mg/ml) and PVP-CL-M (water insoluble; 10 mg/ml). In particular, Figures 9a and 9b, show, respectively, the variation of the liquid-vapor surface tension (γ_{lv}) referring to SLS and TTAB aqueous solution containing K90 or PVP-CL-M. Figure 9a reveals that the presence of K90 sensibly alters the trend of γ_{lv} versus the molar concentration of SLS. This means that there is an interaction between K90 and SLS. On the contrary, as the presence of PVP-CL-M does not affect the trend of γ_{lv} versus the concentration of SLS, we can conclude that interaction between SLS and PVP-CL-M is negligible. Figure 9b, conversely, demonstrates that the interaction between TTAB and K90 or PVP-CL-M is negligible (no modification of the γ_{lv} trend versus TTAB molar concentration). Despite both SLS and TTAB demonstrated to sensibly reduce the water contact angle on nimesulide (69.5 ± 9) when added to water at 1% (w/w) (θ_{SLS} = 21 ± 2; θ_{TTAB} = 22 ± 2), in the light of the above consideration and those relative to the surfactant-polymer films, we decided to explore the effect of SLS on nimesulide release kinetics from nimesulide/PVP-CL-M/SLS co-ground systems (11:32:1 w/w). It is worth underlying that in this ternary system, the SLS mass fraction relative to the PVP/SLS system is 3%, i.e., the minimum surfactant mass fraction ensuring the maximum effect of surfactant (see Figure 8).

Figure 10 shows the release kinetics relative to five different delivery systems. Gray line, representing the release kinetics (dissolution) of pure nimesulide, shows that nimesulide concentration is very low and only after, about, 13 minutes it can be detected. Correctly, nimesulide concentration in the release environment (C_r) never exceeds the water solubility that is 9 μg/ml[5].

Dashed thin line shows the behavior competing to the physical mixture composed by nimesulide/PVP-CL-M. It is evident that the addition of the polymer, although cross-linked and, thus, insoluble, can considerably increase the release kinetics (this effect has been observed also for many other crosslinked polymers). Accordingly, after 20 minutes, C_r approaches nimesulide solubility. Correctly, the physical mixture obtained by adding SLS to nimesulide and PVP-CL-M shows a higher release kinetics (dotted thick line). Indeed, nimesulide dissolution takes now advantage not only by the pres-

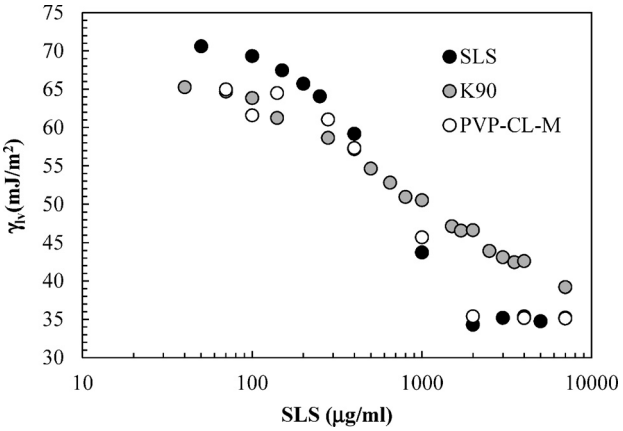

F i g . 9 a – *Variation of the liquid-vapor surface tension (γ_{lv}) referring to pure SLS aqueous solutions (black circles) and to SLS aqueous solutions containing K90 (gray circles) or PVP-CL-M (white circles) at a concentration of 10 mg/ml*

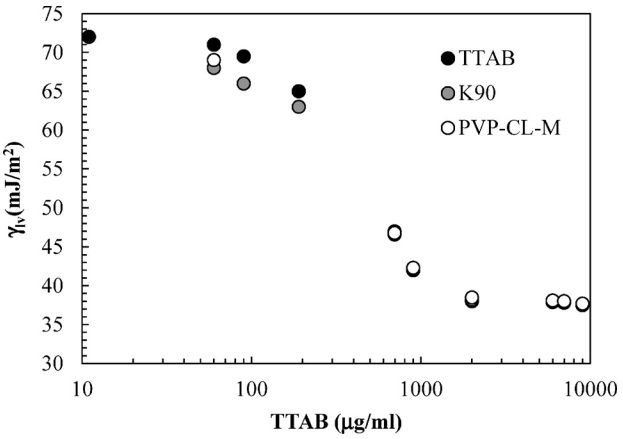

F i g . 9 b – *Variation of the liquid-vapor surface tension (γ_{lv}) referring to pure TTAB aqueous solutions (black circles) and to TTAB aqueous solutions containing K90 (gray circles) or PVP-Clm (white circles) the scarce wettability*

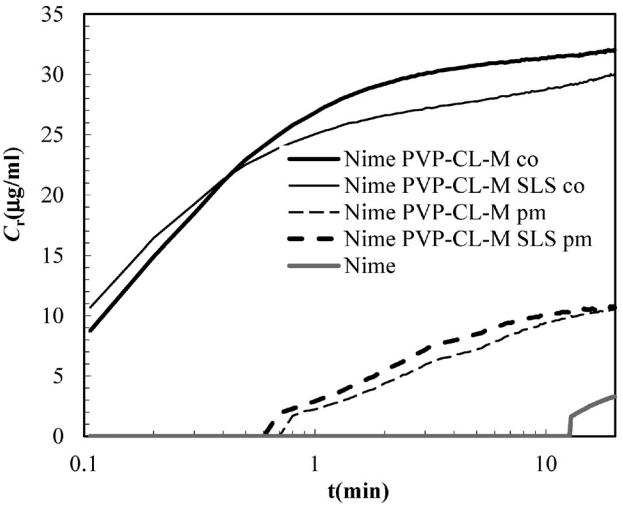

F i g . 1 0 – *Release kinetics relative to the five different delivery systems studied. C_r is the nimesulide concentration in the release environment, while t is time*

ence of the polymer but also by the presence of the surfactant. It is clearly evident that when the physical mixtures made up by nimesulide/PVP-CL-M and by nimesulide/PVP-CL-M/SLS undergo co-grinding, the release kinetics is enormously increased (thick and thin continuous lines, respectively). The differences existing among these two release patterns can be explained in terms of surface and bulk properties. Indeed, the presence of SLS, increasing system wettability, reflects into a higher release kinetics up to 40 seconds. Then, nimesulide/PVP-CL-M exhibits a higher release kinetics. This can be explained reminding that, in this system, nimesulide is present only in nano-crystalline or amorphous form (as demonstrated by DSC analysis, data not shown) and it is well known that nano-crystalline or amorphous drug are associated to higher solubility[4,5,7]. On the contrary, in the nimesulide/PVP-CL-M/SLS system, part of the drug is still present in the original macro-crystals (as demonstrated by DSC analysis, data not shown). As macro-crystals solubility is considerably lower than that competing to nano-crystals and amorphous drug, the global driving force governing the release kinetics is smaller than that competing to nimesulide/PVP-CL-M.

Finally, Figures 11 shows a picture of the nimesulide/PVP-CL-M/SLS system after 2h co-grinding. It is possible to distinguish the small acicular nimesulide crystals from the polymer-surfactant globular structures.

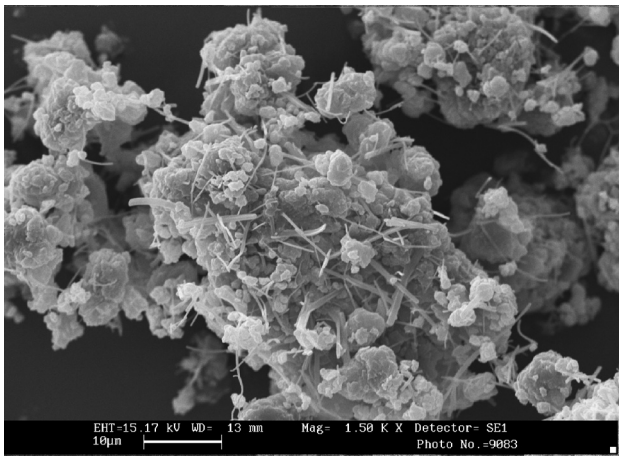

Fig. 11 – *SEM picture of the nimesulide/PVP-CL-M/SLS after 2h co-grinding*

Conclusions

This paper proves that the addition of a proper surfactant can enhance the performance of co-ground drug-polymer systems reducing the problems connected with system wettability. Obviously, apart from other important aspects (drug solubility, particle size distribution and so on), the release kinetics depends not only on surface properties (wettability) but also on bulk properties (drug status: macro-crystals, nano-crystals or amorphous). At this purpose, the surface properties play a more and more important role when the drug amount increases. Typically, wettability can be a rate limiting factor when the drug/polymer ratio is ≥ 1/3. Of course this is not a general rule as this threshold depends on the wettability of the drug. In general, this limit is sound for drug characterized by a contact angle with water around 70°.

The selection of the proper surfactant requires the study of both the bulk and surface properties of the polymer-surfactant system. Typically, DSC and X rays are useful techniques to study bulk properties as they allow determining the solubility of the surfactant in the polymer. Conversely, contact angle measurement is fundamental for the determination of the polar and dispersional components of the solid-vapor surface tension jointly with the excess of polymer and drug at the solid-vapor interface.

References

1. *H. van de Waterbeemd*, in: *J.B. Dressman, H. Lennernäs* (Eds.), Oral Drug Absorption, Prediction and Assessment, Dekker, New York/Basel, 2000, Chap. 4.
2. *Quintavalle U., Voinovich D., Perissutti B., Serdoz F., Grassi G., Dal Col A., Grassi. M*., Eur. J. Pharm. Sci. **33** (2008), 282.
3. Pharmacos 4, Eudralex Collection, Medicinal Products for Human Use: Guidelines. Volume 3C, p. 234.
4. *Amidon, G.L., Lennernas H., Shah V.P., Crison J.R*., Pharm. Res. **12** (1995) 413.
5. *Coceani N., Magarotto L., Ceschia D., Colombo I., Grassi M*., Chem. Eng. Sci. **71** (2012) 345.
6. *Grassi M., Colombo I., Lapasin, R.*, J. Contr. Rel., **68** (2000) 97.
7. *Murdande S. B., Pikal, M. J., Shanker, R. M., Bogner R. H*., J. Pharm. Sci. **99** (2010) 1254.
8. *Nogami H., Nagai T., Yotsuyanagi T*., Chem. Pharm. Bull. **17** (1969) 499.
9. *Grassi G., Hasa D., Voinovich D., Perissutti B., Dapas B., Farra R., Franceschinis E., Grassi M*., Mol. Pharm. **7**(5) (2010) 1488.
10. *Carli F., Colombo I., Magarotto L., Torricelli C.*, Int. J. Pharm. **33** (1986) 115.
11. *Debenedetti P.G., Tom J.W., Yeo S.D., Lim G.B*. J. Contr. Rel. **24** (1992) 27.
12. *Kikic I., Lora M., Cortesi A*., Sist P. Fluid Phase Equilibria, **158–160** (1999) 913.
13. *Colombo I., Grassi G., Grassi M*. J. Pharm. Sci. **98** (2009) 3961.
14. *Voinovich D., Perissutti B., Grassi M., Passerini N., Bigotto A*. J. Pharm. Sci. **98** (2009) 4119.
15. *Hasa, D., Voinovich D., Perissutti B., Bonifacio A., Grassi M., Franceschinis E., Dall'acqua S., Speh M., Plavez J., Invernizzi S*., J. Pharm. Sci. **100** (2011) 915.

16. *Lee P. I.*, Polymer **25** (1984) 973.
17. *Lee P. I.*, J. Contr. Rel. **4** (1986) 1.
18. *M. Grassi, G. Grassi, R. Lapasin, I. Colombo*. Understanding drug release and absorption mechanisms: a physical and mathematical approach", CRC Press, Boca Raton (FL, USA), 2007, 1–627.
19. American Pharmaceutical Association: Handbook of Pharmaceutical Excipients (II ed), pages 448–450, 352–354, and 375–378.
20. *M. I. Ash*: Handbook of Industrial Surfactants, (III ed), Synapse Information Resources, Inc, 1218.
21. *De Simone I.*, Studio dell'interazione polimero-tensioattivo per l'incremento della baganabilità di sistemi polimerici attivati per uso orale, Graduating thesis, Department of Pharmaceutical Sciences, 2003.
22. *Adamson A. W., Gast, A. P.*, "Physical Chemistry of Surfaces", 4th ed., Wiley, New York, 1997.
23. *Kwok D. Y., Neumann, A. W.*, Advances in Colloid and Interface Science **81** (1999) 167.
24. *Wu S. J.*, Polym. Sci., part C, **34** (1971) 19.
25. *Prausnitz J.M., Lichtenthaler R.N., Azevedo E.G.*, 1999. Molecular Thermodynamics of Fluid-Phase Equilibria, third ed. Prentice Hall, Englewood Cliffs, N.J.
26. *Goddard E. D.*, J. Soc. Cosmes. Chem., **41** (1990) 23.
27. *Burgio N., Iasonna A., Magini M., Martelli S., Padella F.*, Il Nuovo Cimento **13 D** (1991) 459.